RSC Advances

PAPER

View Article Online
View Journal | View Issue

Check for updates

Cite this: *RSC Adv.*, 2018, **8**, 21728

Atomic oxygen effects on silvered polyimide films and their surface modification by poly(siloxane amic acid) ammonium salts

Wang Chunbo,[ab] Li Liaoliao,[c] Jiang Haifu,[d] Tian Dongbo,[d] Qin Wei,[d] Liu Changwei,[c] Zhao Xiaogang,[ab] Chen Chunhai [ab] and Wang Daming *[ab]

The tolerance of silvered polyimide films synthesized by an *in situ* self-metalization method against atomic oxygen (AO) was evaluated. The results showed that the mass loss of R–Ag/PI was markedly increased as the AO fluence increased; Ag/PI showed an identical trend. SEM data showed that the silver particles on the surfaces of R–Ag/PI and Ag/PI disappeared. The surfaces achieved a "carpet condition" that was more obvious as the AO fluence increased. Poly(siloxane amic acid) ammonium salt was synthesized and made *via* imidization to produce a flexible organic coating that was characterized by ATR-FTIR, ^{1}HNMR, TGA, and XPS. This could be used to improve the tolerance of silvered polyimide films against AO. The AO resistance and the impacts on mass loss, surface morphology, and surface compositions were also evaluated after surface modification by poly(siloxane amic acid) ammonium salts. 20 wt% Foc/Ag/PI had a lower mass loss and smoother surface than the others due to the formation of a compact surface-SiO_2-type layer. This flexible organic coating can be produced *via* an environmentally-friendly method, and it maintains the inherent thermal stability of the polyimide which cannot be achieved by other anti-AO coatings.

Received 18th April 2018
Accepted 25th May 2018

DOI: 10.1039/c8ra03331e

rsc.li/rsc-advances

Open Access Article. Published on 13 June 2018. Downloaded on 7/6/2025 6:07:07 PM.
This article is licensed under a Creative Commons Attribution-NonCommercial 3.0 Unported Licence.

1 Introduction

Polyimide (PI) is an important class of polymer with superior thermal stability, outstanding electrical properties, excellent mechanical properties, inertness to solvents and good adhesion properties. It has been applied in many fields, such as aerospace, functional membranes, microelectronics, and advanced composites.[1–5] Silvered polyimide films are functional polymers that have been an active area of interest for an *in situ* self-metalization method. They have potential applications in highly reflective thin film reflectors and concentrators in space environments for solar thermal propulsion and large-scale radio frequency antennas.[6–9]

Numerous spacecraft, including the International Space Station (ISS) and Hubble Space Telescope (HST), are running in low-earth orbits (LEOs). In LEO, factors such as atomic oxygen (AO), ultraviolet (UV), ionizing radiation, thermal cycles, and orbital debris can degrade the polymers.[10–13] AO is one of the harshest environmental factors, and it erodes exposed materials.[14–16] Hence, before silvered polyimide films can be used in LEO, evaluation of the tolerance of silvered polyimide films against AO is necessary.[17,18] Silver is prone to erosion by AO, and the primary mechanism is oxidation by atomic oxygen to form porous silver oxide.

Coatings are a common approach to improving the AO resistance of materials.[16] Flexible organic coatings can avoid the defects of hard inorganic coatings that affect AO resistance. These very fragile defects are generated during production. Flexible organic coatings can offer excellent AO erosion resistance and properties that are particularly important for long-term space applications.[19,20]

Here, we evaluated the tolerance of silvered polyimide films synthesized by an *in situ* self-metalization method against AO. Surface modification by poly(siloxane amic acid) ammonium salts (PAAS) made by imidization produced flexible organic coatings. We also evaluated the AO resistance after surface modification by poly(siloxane amic acid) ammonium salts at different solid contents. The metrics include mass loss, surface morphology and surface composition.

2 Experimental

2.1 Materials

Commercial Kapton polyimide films (Dupont, 50 μm) were used. Potassium hydroxide (KOH), silver nitrate ($AgNO_3$), ethanol,

[a]*Key Laboratory of High Performance Plastics (Jilin University), Ministry of Education, College of Chemistry, Jilin University, Changchun, 130012, P. R. China. E-mail: wangdaming@jlu.edu.cn*

[b]*National & Local Joint Engineering Laboratory for Synthesis Technology of High Performance Polymer, College of Chemistry, Jilin University, Changchun, 130012, P. R. China*

[c]*Institute of Petroleum Chemistry, Heilongjiang Academy of Sciences, Harbin 150040, China*

[d]*Beijing Institute of Satellite Environment Engineering, Beijing 100094, China*

This journal is © The Royal Society of Chemistry 2018

Open Access Article. Published on 13 June 2018. Downloaded on 7/6/2025 6:07:07 PM.
This article is licensed under a Creative Commons Attribution-NonCommercial 3.0 Unported Licence.

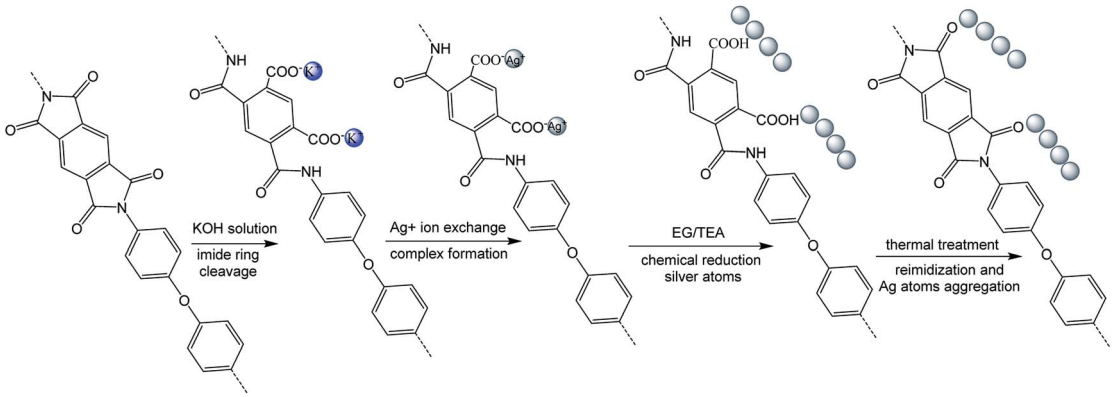

Scheme 1 Preparation of the self-metalized films.

triethylamine (TEA), and ethylene glycol (EG) were purchased from Acros and used without further purification. Bis(γ-aminopropyl) polydimethylsiloxane (M_n = 860 g mol^{-1}) was supplied by Gelest Inc., and was used as received. 3,3′,4,4′-Biphenyltetracarboxylic dianhydride was purchased from Sinopharm Chemical Reagent Beijing Co. Ltd and baked at 110 °C in a vacuum overnight prior to use.

2.2 Characterization

^{1}H nuclear magnetic resonance (NMR) spectra were measured on a BRUKER-300 spectrometer at 300 MHz. Thermogravimetric analysis (TGA) was tested with a TA 2050 at a heating rate of 10 °C min^{-1} under air. The surface composition and surface chemical states were measured *via* X-ray photoelectron spectroscopy (XPS) by using an Escalab 250. The AO irradiation tests were performed using a microwave source AO ground simulation device, and a typical AO flux was estimated to be 2.5 × 10^{14} atoms per (cm^2 s). Samples were weighed using an electronic balance (AB135-S, METTLER TOLEDO) at room temperature immediately after the AO irradiation tests. The mass of the sample was taken as the average of three measurements. Mass loss was defined as the difference in value of the mass before and after exposure to AO. The AO-irradiated sample surfaces were observed using scanning electron microscopy (SEM, NOVA NANOSEM 450, England). Samples used for surface morphology observation were deposited on *ca.* 5 nm platinum (Pt) prior to measurement.

2.3 Preparation of the self-metalized films[8]

First, polyimide films (Kapton, 50 μm) were immersed into aqueous KOH solution (4 M) for 15 minutes at room temperature and then washed with lots of deionized water. Second, the silver ions were incorporated into the surface-modified films *via* aqueous $AgNO_3$ solution (1 M) for 1 h at room temperature. The film was then washed with deionized water. Third, the silver ions were reduced by immersion of the films into the solution (EG : TEA = 10 : 1) for 5 minutes at 90 °C. The surface-modified films were obtained after reduction and named R–Ag/PI.

Finally, R–Ag/PI was made by reimidization *via* thermal treatment (100 °C/1 h; 200 °C/1 h; 300 °C/1 h) to obtain the surface-modified films after reimidization, and named Ag/PI (see Scheme 1).

2.4 Preparation of poly(siloxane amic acid) ammonium salt (PAAS)[21]

1.47 g of 3,3′,4,4′-biphenyltetracarboxylic dianhydride was slowly added to the solution of bis(γ-aminopropyl)polydimethylsiloxane (4.30 g, 5 mmol) in 41 ml of ethanol. Then, the reaction mixture was stirred at −10 °C for 10 h under N_2 protection. Subsequently, 1.01 g of triethylamine was added slowly (0.5–1 h), and the reaction mixture was stirred for another 4 h. After drying under vacuum at 40–50 °C overnight, poly(siloxane amic acid) ammonium salt (PAAS) was obtained (see Scheme 2).

2.5 Surface modification of Ag/PI by PAAS

PAAS was dissolved in ethylene glycol with a little triethylamine at solid contents of 10 and 20 wt%, respectively. Then, the solutions were spun on the surface of R–Ag/PI. The flexible organic coatings were obtained after imidization (100 °C/1 h; 200 °C/1 h; 300 °C/1 h) and named 10 wt% Foc/Ag/PI and 20 wt% Foc/Ag/PI (see Scheme 3).

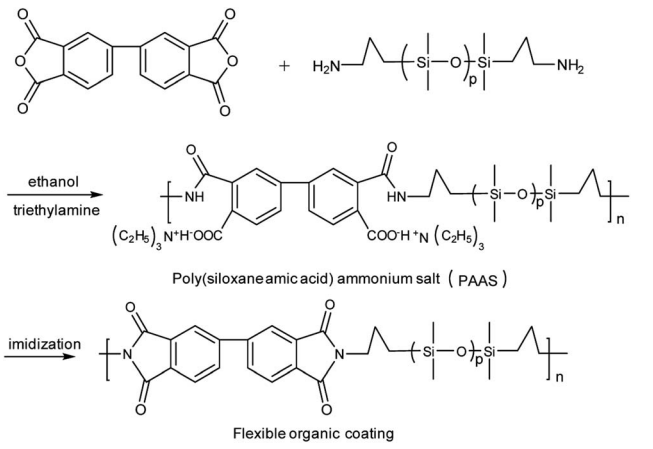

Scheme 2 Synthesis of PAAS and imidization to obtain flexible organic coatings.

Open Access Article. Published on 13 June 2018. Downloaded on 7/6/2025 6:07:07 PM.
This article is licensed under a Creative Commons Attribution-NonCommercial 3.0 Unported Licence.

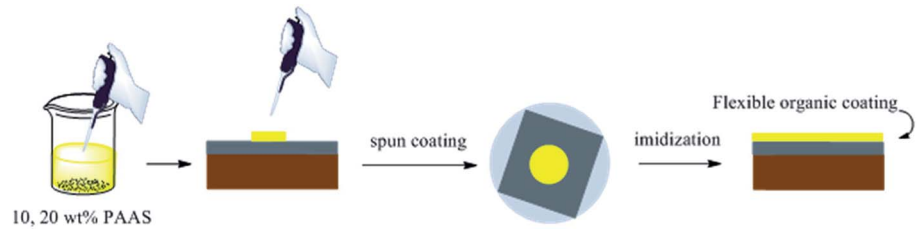

Scheme 3 Surface modification of the self-metalized films by PAAS.

3 Results and discussion

3.1 Preparation of the samples

Many groups have reported the primary mechanism of the self-metalized reaction on the polyimide surface. Here, a self-metalized film was prepared *via* the procedures of hydrolytic cleavage of the imide groups, incorporation of silver ions, reduction of silver ions and reimidization (see Scheme 1). The depth of the surface-modified film was *ca.* 5 μm, as measured by SEM *via* fracture morphology. The XPS results showed the bonding states of the silver on the surface of R–Ag/PI and Ag/PI. These were characteristic of metallic silver with peaks located at binding energies around 368.4 eV (see Fig. 3).[22]

Compared to poly(amic acid), poly(amic acid) ammonium salt has hydrolytic stability and good solubility in some environmentally-friendly solvents.[23] Meanwhile, polysiloxane-*block*-polyimides possess good AO resistance, as reported in the literature.[20] Therefore, poly(siloxane amic acid) ammonium salts were synthesized and spun on the surface of R–Ag/PI at solid contents of 10 wt% and 20 wt%, and then imidized: 100 °C/1 h; 200 °C/1 h; 300 °C/1 h (see Schemes 2 and 3) to obtain a flexible organic coating that can protect the silvered polyimide from AO attack. ATR-FTIR measurements were performed on 10 wt% Foc/Ag/PI and 20 wt% Foc/Ag/PI, as shown in Fig. 1.

For the flexible organic coating, a relatively strong peak attributed to the Si–O stretching of the siloxane appeared at 1016 and 1063 cm^{-1}. The characteristic bands for the imide groups appeared at 1770, 1710 cm^{-1}, and 1380 cm^{-1}. This proved that PAAS formed polyimide. The absence of the characteristic peaks of PAAS at about 1660 cm^{-1} (amic acid C=O stretching) and 1535 cm^{-1} (amide C–N stretching) suggest complete imidization of PAAS. The flexible organic coating derived from $-CH_3$ absorption had a peak at 2960 cm^{-1} and Si–CH_3 absorption was at 794 and 841 cm^{-1}. ^1H NMR was measured on a flexible organic coating, as shown in Fig. 2 (^1H NMR (400 MHz, $CDCl_3$) δ 8.08 (s, 2H), 7.95 (s, 4H), 3.69 (t, J = 6.7 Hz, 4H), 1.71 (s, 4H), 0.62–0.54 (m, 4H), 0.22–0.00 (m, 84H)). The signals at δ 8.08 and 7.95 are derived from benzene; signals of the propyl group appeared at δ 3.69, 1.71 and 0.62–0.54; the relatively strong peak at 0.22–0.00 was attributed to the methyl connecting with the silicon. The spectroscopic data obtained by ^1H NMR and ATR-FTIR agreed with the expected structures.

After surface modification by PAAS, the silver contents on the surfaces of 10 wt% Foc/Ag/PI and 20 wt% Foc/Ag/PI decreased from 25.63% and 20.46% to 2.08% and 0%, in Fig. 3 and 4. This data showed that the silver cannot be completely covered *via* surface modification with a solid content of 10 wt% PAAS. However, surface modification with 20 wt% PAAS left no silver on the surface.

3.2 Thermal stability of the samples

TGA curves of the samples: (a) R–Ag/PI; (b) Ag/PI; (c) 10 wt% Foc/Ag/PI; (d) 20 wt% Foc/Ag/PI are listed in Fig. 5, and the decomposition temperature (T_d) at 10% weight loss in an air atmosphere was determined from the original TGA curves and

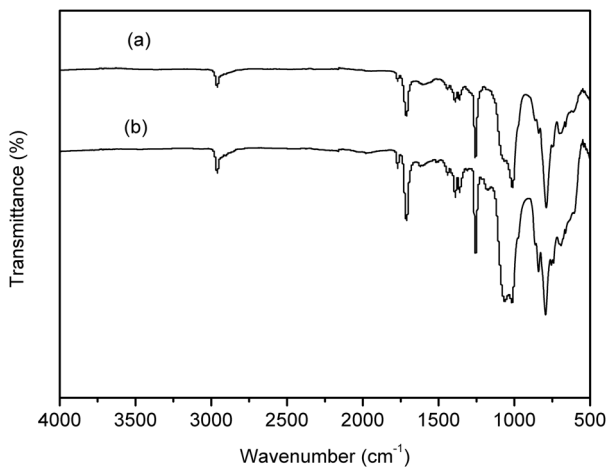

Fig. 1 ATR-FTIR spectra of (a) 10 wt% Foc/Ag/PI and (b) 20 wt% Foc/Ag/PI.

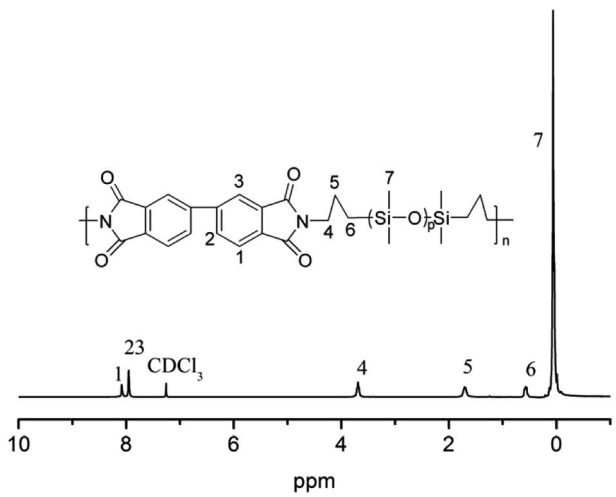

Fig. 2 ^1H NMR spectrum of the flexible organic coating.

This journal is © The Royal Society of Chemistry 2018

Open Access Article. Published on 13 June 2018. Downloaded on 7/6/2025 6:07:07 PM.
This article is licensed under a Creative Commons Attribution-NonCommercial 3.0 Unported Licence.

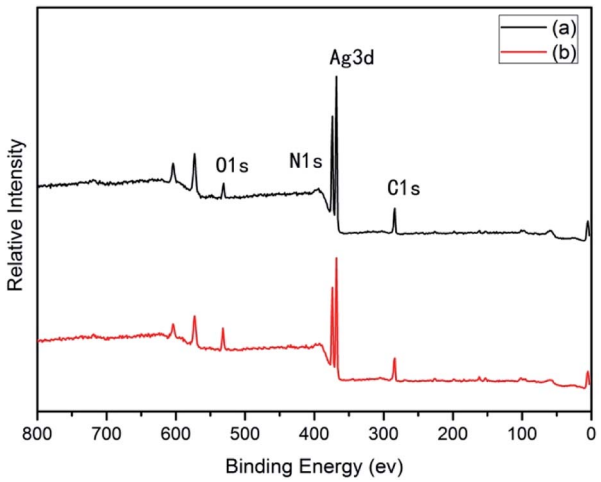

Fig. 3 XPS spectra of the samples: (a) R–Ag/PI; (b) Ag/PI.

is also given in Table 1. The 10% weight loss temperatures ($T_{10\%}$) of R–Ag/PI and Ag/PI in air were recorded at 409 and 518 °C. Thermogravimetric analysis of the R–Ag/PI film shows some mass loss around 200–250 °C due to the existence of residual solvent and amic acids. After reimidization, the Ag/PI had no mass loss under 400 °C. The 10% weight loss temperatures were markedly increased after reimidization (R–Ag/PI *versus* Ag/PI). Hence, it is necessary that the surface-modified films after reduction be reimidized to improve the thermal stability of the self-metalized films. The 10% weight loss temperatures ($T_{10\%}$) of 10 wt% Foc/Ag/PI and 20 wt% Foc/Ag/PI in air were recorded at 445 and 436 °C, respectively. The 10% weight loss temperatures obviously decreased after surface modification by PAAS, but they also had outstanding thermal stability compared with other organic silicon resins. A slight mass loss at around 200–250 °C was seen with imidization for 10 wt% Foc/Ag/PI and 20 wt% Foc/Ag/PI. This is because PAAS was spun on the surface of R–Ag/PI, and the protective layer may hinder the volatilization of the solvent existing in the substrate.

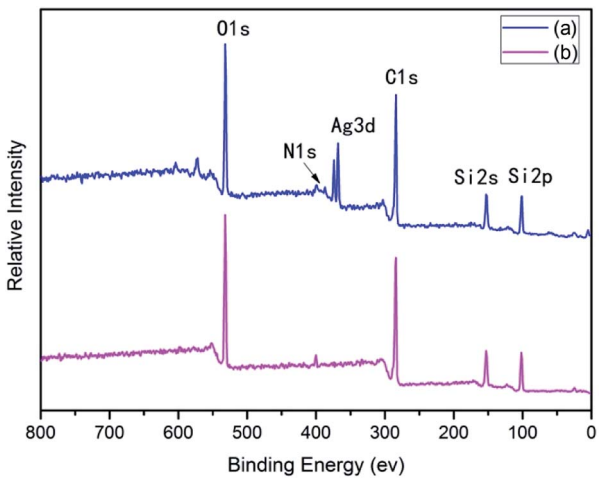

Fig. 4 XPS spectra of the samples: (a) 10 wt% Foc/Ag/PI; (b) 20 wt% Foc/Ag/PI.

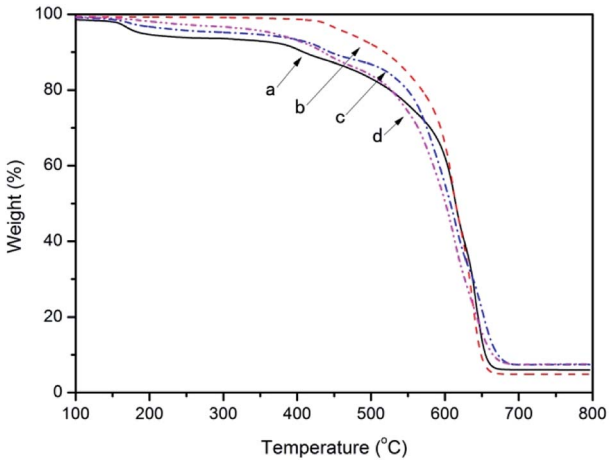

Fig. 5 TGA curves of the samples: (a) R–Ag/PI; (b) Ag/PI; (c) 10 wt% Foc/Ag/PI; and (d) 20 wt% Foc/Ag/PI.

3.3 Surface morphology of the samples

SEM data: (a) R–Ag/PI; (b) Ag/PI; (c) 10 wt% Foc/Ag/PI; (d) 20 wt% Foc/Ag/PI are shown in Fig. 6. A number of silver particles on the R–Ag/PI and Ag/PI surfaces were observed, and well-defined silver layers formed after re-imidization. The SEM pictures of 10 wt% Foc/Ag/PI and 20 wt% Foc/Ag/PI show that 10 wt% PAAS cannot fully cover the silver layers on the surface of self-metalized films, but silver particles cannot be seen after modification by 20 wt% PAAS. This phenomenon can also be illustrated with XPS data.

Table 1 $T_{10\%}$ of the samples derived from TGA curves

Samples	$T_{10\%}$ (°C)
R–Ag/PI	409
Ag/PI	518
10 wt% Foc/Ag/PI	445
20 wt% Foc/Ag/PI	436

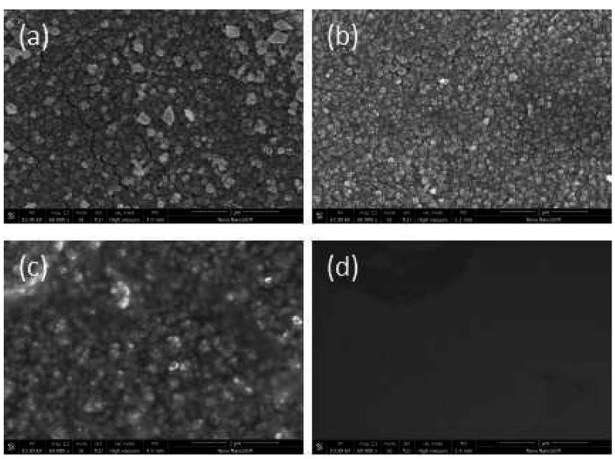

Fig. 6 SEM pictures of the samples: (a) R–Ag/PI; (b) Ag/PI; (c) 10 wt% Foc/Ag/PI; (d) 20 wt% Foc/Ag/PI.

Open Access Article. Published on 13 June 2018. Downloaded on 7/6/2025 6:07:07 PM.
This article is licensed under a Creative Commons Attribution-NonCommercial 3.0 Unported Licence.

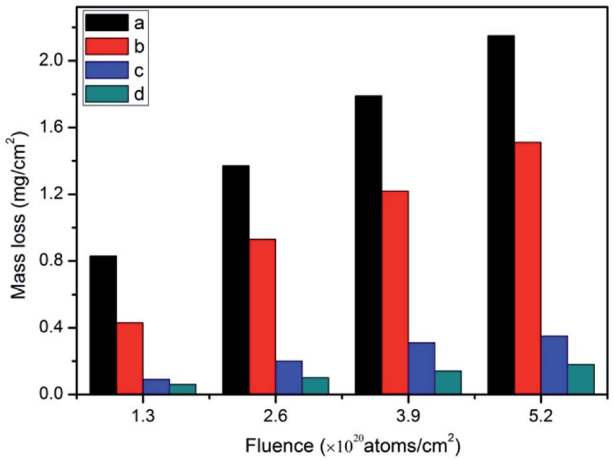

Fig. 7 Mass loss of the samples: (a) R–Ag/PI; (b) Ag/PI; (c) 10 wt% Foc/Ag/PI; and (d) 20 wt% Foc/Ag/PI.

3.4 AO resistance

3.4.1 Mass loss. Mass loss data: (a) R–Ag/PI; (b) Ag/PI; (c) 10 wt% Foc/Ag/PI; (d) 20 wt% Foc/Ag/PI at different fluences are listed in Fig. 7. The average mass losses of R–Ag/PI at each AO fluence of 1.3×10^{20}, 2.6×10^{20}, 3.9×10^{20}, and 5.2×10^{20} atoms per cm^2 were 0.83, 1.37, 1.79, and 2.15 mg cm^{-2}, respectively. The mass losses of R–Ag/PI increased markedly as the AO fluence increased. Ag/PI showed an identical trend. However, the mass loss of Ag/PI was slightly decreased compared with R–Ag/PI, which might be because of the well-established silver layers after reimidization resulting in a loose porous silver oxide layer that fell off. The mass loss of Ag/PI at an AO fluence of 5.2×10^{20} atoms per cm^2 was 1.51 mg cm^{-2}.

The mass losses of 10 wt% Foc/Ag/PI and 20 wt% Foc/Ag/PI were markedly reduced compared with R–Ag/PI and Ag/PI. This was the result of modification by PAAS. They showed the same trend as R–Ag/PI as AO fluence increased. The average mass losses of 10 wt% Foc/Ag/PI and 20 wt% Foc/Ag/PI at an AO fluence of 5.2×10^{20} atoms per cm^2 were 0.35 and 0.18 mg cm^{-2} 20 wt% Foc/Ag/PI had a lower mass loss than 10 wt% Foc/Ag/PI, because 10 wt% PAAS cannot fully cover the silver layers on the surface of self-metalized films. This can be seen in the SEM and XPS data.

3.4.2 Surface morphology change. SEM pictures of the samples are listed in Fig. 8: (a)–(d) R–Ag/PI at fluences of 1.3, 2.6, 3.9, and 5.2×10^{20} atoms per cm^2, respectively; (e)–(h) Ag/PI at fluences of 1.3, 2.6, 3.9, and 5.2×10^{20} atoms per cm^2,

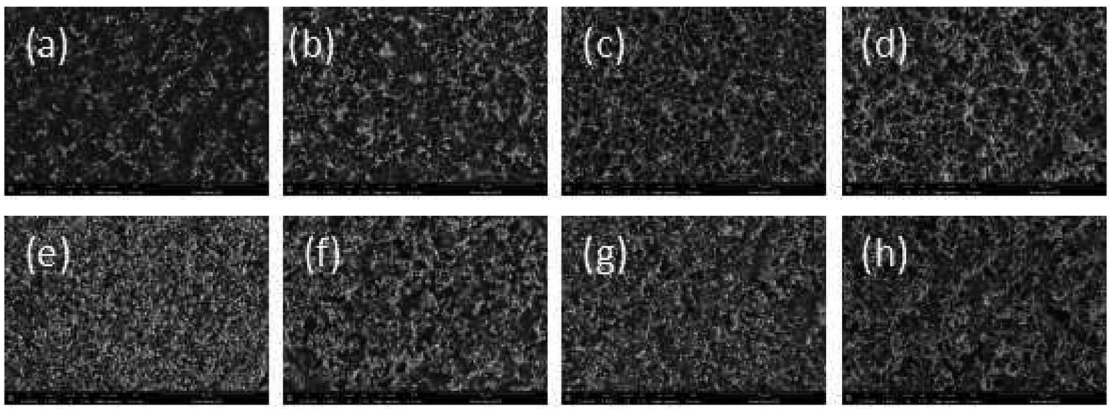

Fig. 8 SEM pictures of the samples: (a)–(d) R–Ag/PI at fluences of 1.3, 2.6, 3.9 and 5.2×10^{20} atoms per cm^2, respectively; (e)–(h) Ag/PI at fluences of 1.3, 2.6, 3.9 and 5.2×10^{20} atoms per cm^2, respectively.

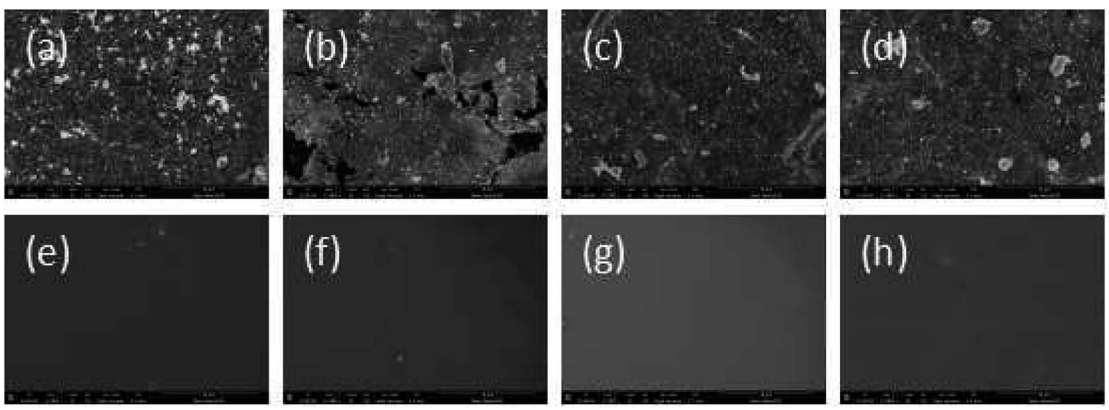

Fig. 9 SEM pictures of the samples: (a)–(d) 10wt% Foc/Ag/PI; (e)–(h) 20wt% Foc/Ag/PI at fluences of 1.3, 2.6, 3.9, and 5.2×10^{20} atoms per cm^2, respectively.

This journal is © The Royal Society of Chemistry 2018

Open Access Article. Published on 13 June 2018. Downloaded on 7/6/2025 6:07:07 PM.
This article is licensed under a Creative Commons Attribution-NonCommercial 3.0 Unported Licence.

Table 2 Surface atomic concentration (in percent) determined from XPS survey scans before and after AO exposure to a fluence of 5.2×10^{20} atoms per cm^2

Materials		At% C1s	N1s	O1s	Ag3d	Si2p
R–Ag/PI	Before AO	51.04	9.11	14.23	25.63	—
	After AO	59.94	5.05	21.81	12.66	—
Ag/PI	Before AO	53.67	6.48	19.39	20.46	—
	After AO	57.85	6.75	23.80	11.11	—
10 wt% Foc/Ag/PI	Before AO	53.60	3.16	22.48	2.08	18.73
	After AO	35.50	7.11	29.31	13.61	12.53
20 wt% Foc/Ag/PI	Before AO	55.24	3.36	22.33	—	19.07
	After AO	41.88	17.34	25.22	0.35	9.43

respectively. SEM showed fewer silver particles on the surfaces of R–Ag/PI and Ag/PI after exposure to AO. The surfaces attained a "carpet condition" that was more obvious as the AO fluence increased. This might be because silver particles were oxidized by AO to form silver oxide that became loose and fell off.

The surface morphology change was also measured after surface modification by PAAS. SEM data of the samples are shown in Fig. 9: (a)–(d) 10 wt% Foc/Ag/PI at fluences of 1.3, 2.6, 3.9, and 5.2×10^{20} atoms per cm^2, respectively; (e)–(h) 20 wt% Foc/Ag/PI at fluences of 1.3, 2.6, 3.9, and 5.2×10^{20} atoms per cm^2, respectively. After exposure to AO, the surface morphology on 10 wt% Foc/Ag/PI was distinctly improved compared to Fig. 8. However, the surface also had some conspicuous drawbacks that will affect the properties of the self-metalized films. 20 wt% Foc/Ag/PI had a smooth surface at fluences of 1.3, 2.6, 3.9, and 5.2×10^{20} atoms per cm^2. This might be attributed to full coverage over the self-metalized films by PAAS, and a compact protective layer coming into being after exposure to AO. The protective layer structure is confirmed in Section 3.4.3.

3.4.3 Surface compositional and structural change. Surface atomic concentrations (in percent) determined from XPS survey scans before and after AO exposure to a fluence of 5.2×10^{20} atoms per cm^2 are summarized in Table 2. For R–Ag/PI and Ag/PI, the concentration of the irradiated-surface silver atoms dramatically decreased to almost half compared to that of the pristine samples. This phenomenon was due to the reaction of silver on the surface with AO to form a loosened silver oxide that became detached. The concentration of the irradiated-surface silver atoms on 10 wt% Foc/Ag/PI increased from 2.08% to 13.61%, and this might be because the uncovered silver oxide did not detach because of the existence of a sparse protective layer derived from 10 wt% Foc/Ag/PI. The concentration of the irradiated-surface silver atoms on 20 wt% Foc/Ag/PI was only 0.35%.

A protective layer structure was confirmed by high-resolution XPS spectra (see Fig. 10 and 11). The Si2p peak position for the pristine surfaces was located at *ca.* 102.0 eV, belonging to the O–Si–O in the siloxane. However, the Si2p peak after AO exposure to a fluence of 5.2×10^{20} atoms per cm^2 was divided into two different shifts located at *ca.* 102.0 and 103.6 eV. The existence of the binding energy of *ca.* 102.0 eV showed that the O–Si–O bonds derived from siloxane did not disappear. However, the presence of a new binding energy at *ca.* 103.6 eV indicated the formation of a surface-SiO_2-type layer. Finally, the passivated SiO_2 layer can prevent surface erosion by AO. Thus, 20 wt% Foc/Ag/PI had a lower mass loss and smoother surface than the others. The erosion and protective mechanism of silvered polyimide films and surface modification by PAAS are depicted in Fig. 12.

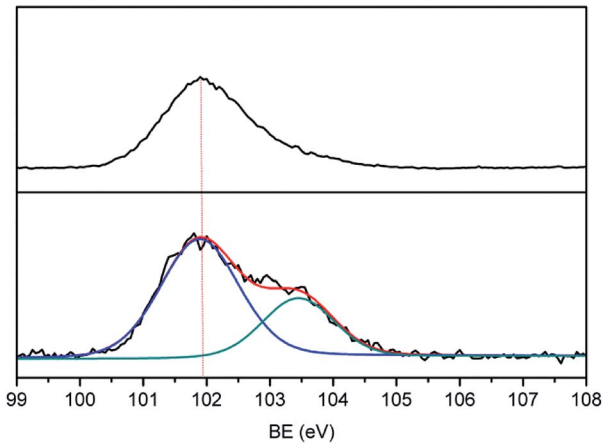

Fig. 11 High-resolution Si2p spectra of 20 wt% Foc/Ag/PI.

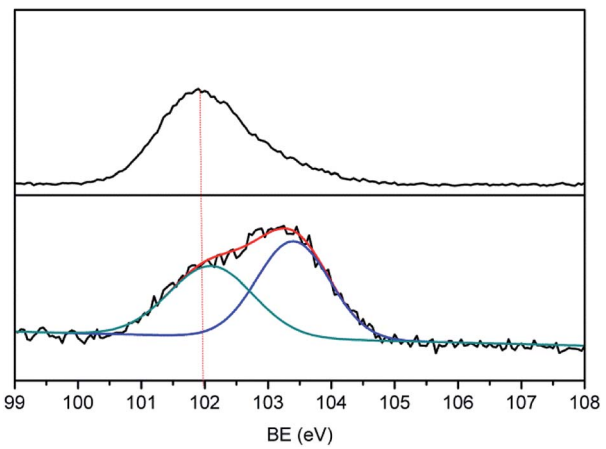

Fig. 10 High-resolution Si2p spectra of 10 wt% Foc/Ag/PI.

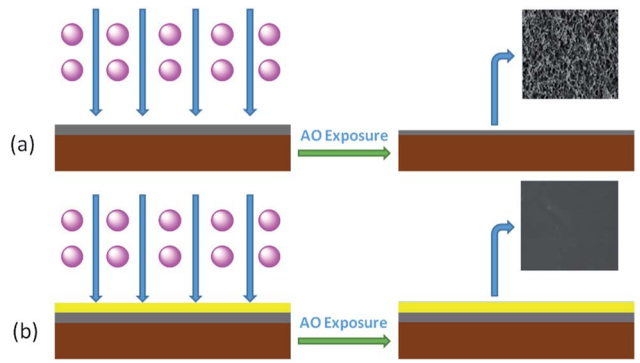

Fig. 12 Schematic of the erosion or protective mechanism: (a) silvered polyimide films and (b) surface modification by PAAS.

Open Access Article. Published on 13 June 2018. Downloaded on 7/6/2025 6:07:07 PM.
This article is licensed under a Creative Commons Attribution-NonCommercial 3.0 Unported Licence.

4 Conclusions

We evaluated the tolerance of silvered polyimide films synthesized by an *in situ* self-metalization method against AO. Mass losses of R–Ag/PI were markedly increased as the AO fluence increased, and Ag/PI showed an identical trend. Compared to SEM pictures before exposure to AO, silver particles on R–Ag/PI and Ag/PI disappeared, and the surfaces attained a "carpet condition" that was more obvious as the AO fluence increased.

After surface modification by poly(siloxane amic acid) ammonium salts, the AO resistance and the impacts on mass loss, surface morphology, and surface compositions were also evaluated. 20 wt% Foc/Ag/PI had the lowest mass loss and the smoothest surface. This was due to the formation of a compact surface-SiO_2-type layer.

Conflicts of interest

There are no conflicts to declare.

Acknowledgements

Financial support from the foundation (JSHS2015203B002) is gratefully acknowledged.

References

1 D. J. Liaw, K. L. Wang, Y. C. Huang, K. R. Lee, J. Y. Lai and C. S. Ha, *Prog. Polym. Sci.*, 2012, **37**, 907–974.
2 X. Ma, R. Swaidan, Y. Belmabkhout, Y. Zhu, E. Litwiller, M. Jouiad, I. Pinnau and Y. Han, *Macromolecules*, 2012, **45**, 3841–3849.
3 K. L. Mittal, *Polyimides and Other High Temperature Polymers: synthesis, characterization, and applications*, Brill, vol. 4, 2007.
4 M. Ghosh, *Polyimides: Fundamentals and Applications*, Belgeler Com, 1996, vol. 2004, ch. xii, p. 404.
5 M. Ding, *Prog. Polym. Sci.*, 2007, **32**, 623–668.
6 J. E. Prussing, *J. Guid. Control Dyn.*, 2004, **23**, 768.
7 R. E. Freeland, G. D. Bilyeu and G. R. Veal, *Acta Astronaut.*, 1996, **38**, 251–260.
8 Z. Wu, D. Wu, S. Qi, Z. Teng and R. Jin, *Thin Solid Films*, 2005, **493**, 179–184.
9 S. Qi, Z. Wu, D. Wu, A. Wencai Wang and R. Jin, *Chem. Mater.*, 2007, **19**, 393–401.
10 A. C. Tribble, *The Space Environment: Implications for Spacecraft Design*, Princeton Univ Pr, 2003.
11 H. Shimamura and T. Nakamura, *Polym. Degrad. Stab.*, 2009, **94**, 1389–1396.
12 N. Atar, E. Grossman, I. Gouzman, A. Bolker, V. J. Murray, B. C. Marshall, M. Qian, T. K. Minton and Y. Hanein, *ACS Appl. Mater. Interfaces*, 2015, **7**, 12047–12056.
13 T. K. Minton, M. E. Wright, S. J. Tomczak, S. A. Marquez, L. Shen, A. L. Brunsvold, R. Cooper, J. Zhang, V. Vij and A. J. Guenthner, *ACS Appl. Mater. Interfaces*, 2012, **4**, 492–502.
14 M. R. Reddy, *J. Mater. Sci.*, 1995, **30**, 281–307.
15 J. W. Connell, J. Smith, G. Joseph, C. G. Kalil and E. J. Siochi, *Polym. Adv. Technol.*, 2015, **9**, 11–19.
16 S. Packirisamy, D. Schwam and M. H. Litt, *J. Mater. Sci.*, 1995, **30**, 308–320.
17 L. Li, J. C. Yang and T. K. Minton, *J. Phys. Chem. C*, 2007, **111**, 6763–6771.
18 M. K. Bhan, P. K. Nag, G. P. Miller and J. C. Gregory, *J. Vac. Sci. Technol., A*, 1994, **12**, 699–706.
19 L. Hu, M. Li, C. Xu and Y. Luo, *Thin Solid Films*, 2011, **520**, 1063–1068.
20 E. Miyazaki, M. Tagawa, K. Yokota, R. Yokota, Y. Kimoto and J. Ishizawa, *Acta Astronaut.*, 2010, **66**, 922–928.
21 D. Cai, J. Su, M. Huang, Y. Liu, J. Wang and L. Dai, *Polym. Degrad. Stab.*, 2011, **96**, 2174–2180.
22 S. CV, A. Cavaleiro and S. Carvalho, *Appl. Surf. Sci.*, 2015, **346**, 240–247.
23 Z. Cao, C. Liu, C. Qu, X. Zhao, D. Wang, C. Chen, X. Hou, L. Li and G. Zhu, *Eur. Polym. J.*, 2017, **96**, 393–402.

This journal is © The Royal Society of Chemistry 2018